Biosensors and Bioelectronics 142 (2019) 111566

Contents lists available at ScienceDirect

Biosensors and Bioelectronics

journal homepage: www.elsevier.com/locate/bios

# Carbon nanotube based dielectric spectroscopy of tumor secretion; electrochemical lipidomics for cancer diagnosis

Ashkan Zandi[a,b,1], Ali Gilani[a,b,1], Fereshteh Abbasvandi[c], Pouyan Katebi[a,b,1], Saeid Rafizadeh Tafti[a,b], Sepanta Assadi[a,b,1], Hassan Moghtaderi[a,b,1], Mohammad Salemizadeh Parizi[a,b], Mohammad Saghafi[a,b], Mohammad Ali Khayamian[a,b], Zahra Davari sh[a,b], Parisa Hoseinpour[d], Masoumeh Gity[e], Hassan Sanati[c], Mohammad Abdolahad[a,b,*,1]

[a] Nano Electronic Center of Excellence, Nanobioelectronic Devices Lab., School of Electrical and Computer Eng., Faculty of Engineering, University of Tehran, P.O. Box 14395/515, Tehran, Iran
[b] Nano Electronic Center of Excellence, Nanoelectronics Lab., School of Electrical and Computer Eng.,Faculty of Engineering, University of Tehran, P.O. Box 14395/515, Tehran, Iran
[c] ATMP Department, Breast Cancer Research Center, Motamed Cancer Institute, ACECR, P.O. BOX 15179/64311, Tehran, Iran
[d] SEPAS Pathology Laboratory, P.O.Box: 1991945391, Tehran, Iran
[e] Advanced Diagnostic and Interventional Radiology Research Center, Tehran University of Medical Sciences, P.O. Box 14155/6447, Tehran, Iran

ARTICLE INFO

*Keywords:*
Electrical impedance sensor
Cellular micro-environment
Lipid secretion
Electrochemical impedance spectroscopy (EIS)
Tumor micro-environment
Cancer diagnose

ABSTRACT

Cell free diagnosis of cancer is one of the crucial fields in new generation of medical technology. In this regard, cancer detection based on coastal fluids secreted from the tissues (named as secretome) has attracted a lot of attention. Lipids are important macromolecules could be found with much higher concentrations in secretome of cancer tissues vs. normal ones. On the other hand, lipids are the main dielectric components of the secretome with respect to proteins and ions. Here for the first time we introduced an electrochemical lipidomics based on electrical impedance spectroscopy (EIS) of the secretomes to detect the cancerous samples due to the lipidic content of their secretions. The EIS sensor was fabricated by multiwall carbon nanotube (MWCNT) arrays as conductive and super hydrophobic materials to have great interactive surface with the lipidic content of the solution. Results of the tests on the secretions of more than 100 human biopsied breast tissues showed the promising match between the charge transfer resistance ($R_{CT}$) of samples' secretions and pathological states of the tissues with meaningful boundary (up to 8 kΩ for normal and more than 13 kΩ for cancer samples). Mass spectroscopic analyses confirmed the higher content of lipids in cancer secretomes. Electrical lipidomics of the secretome shed new lights in cell free cancer diagnosis and could be applied as a complementary clinical approach in all of biopsy based diagnoses in future.

## 1. Introduction

Secretions of tumor cells contain a rich source of cancer associated macromolecules such as proteins (Finicle et al., 2018)(Karagiannis et al., 2010)(Me, 2013), lipids (Beloribi-djefa et al., 2016)(Skotland et al., 2017)(Ackerman and Simon, 2014a)and ionic species (Binnewies et al., 2018)(Peter et al., 2007)' (Bose et al., 2015). Hence, secretome analysis could be so helpful to detect the malignancy (Apicella et al., 2018)(Me, 2013).

Among the secretion components, lipids are one of the crucial cancer associated macromolecules. It is known that cancer is the consequence of an alteration in lipid metabolic enzymes and pathways (Beloribi-djefa et al., 2016). Cancer cells show an increased lipogenesis and lipid secretion to mediate some invasive associated pathways such as angiogenesis (De Palma et al., 2017), immune suppressing (Binnewies et al., 2018)(Nakanishi and Rosenberg, 2013) and chemoresistance (Kurtova et al., 2014). Hence, lipids are now considered as hallmarks of cancer aggressiveness (Beloribi-djefa et al., 2016)(Yue

* Corresponding author. Nano Electronic Center of Excellence, Nanobioelectronic Devices Lab., School of Electrical and Computer Eng., Faculty of Engineering, University of Tehran, P.O. Box 14395/515, Tehran, Iran.
*E-mail address:* m.abdolahad@ut.ac.ir (M. Abdolahad).
[1] Authors with same collaboration.

https://doi.org/10.1016/j.bios.2019.111566
Received 19 May 2019; Received in revised form 31 July 2019; Accepted 2 August 2019
Available online 06 August 2019
0956-5663/ 

et al., 2014) as far as lipid induced facilitation of metastasis becomes interested for cancer biologists (Luo et al., 2018). Many complicated and expensive methods have been developed to analyze the lipid content of cellular secretomes such as liquid chromatography (LC) Mass, marker binding based enzyme linked immunosorbent assay (ELISA) (Chen et al., 2018)(Brügger, 2014) and *etc*. Apart from their chemical structures, lipids are considered as dielectric components in biological media (Gramse et al., 2013). The electrically insulating behavior of the lipids are much stronger than other contents of intercostal and extracellular fluids (Joshi and Maiti, 2018)(Richens et al., 2015) (Nikshoar et al., 2017). Hence, dielectric spectroscopy might be a simple and precise alternative for lipid analysis. Here, a cell-free dielectric spectroscopic method was applied to investigate the concentration of secreted lipids from the breast cell lines as well as biopsied samples from the patients with breast suspicious tumors. Multiwall carbon nanotubes (MWCNTs) as highly conductive nanostructures with super hydrophobic properties (Nicola et al., n.d.) were grown as impedance recording electrodes to make perfect physical and electrical interactions with the lipid component of secretion. In this study, the electrical impedance spectroscopy (EIS) of secretions was quantified and compared with cancerous grades of the samples to find any probable diagnostic correlation between pathological phenotypes of the samples and dielectric parameters of their secretions. Charge transfer resistance ($R_{CT}$) was derived and categorized as quantitative values in lipid based dielectric spectroscopy of the tumor secretome. Matching between pathological states of the tissues and $R_{CT}$ values of their secretomes were investigated on more than 100 patients. This technique, named electrochemical lipidomics, might shed new light in cancer diagnosis as a cell free complementary analysis.

## 2. Results and discussions

### 2.1. Device characterization

Two concepts must be concerned in choosing the electrodes in electrochemical lipidomics of secretion. First, surface hydrophobicity and second, electrical conductance. Hydrophobic surface would apply well physical adhesion with lipid layer. Well electrical conductance of the sensing surface would enhance signal transmission. We candidate the vertically aligned multiwall carbon nanotube (VA-MWCNT) array as a famous nanostructure in bioelectrical sensing approaches [16,] (Zhu et al., 2012)' (Zhu, 2017).

Fig. 1.a presented the schematic operation of the system. The device was fabricated by photolithography (See methods) and covered by grown MWCNTs. Super hydrophobic surface of CNT electrodes was revealed through analyzing by contact angle method (Fig. 1b). The lipid free droplet of culture media, Dulbecco's Modified Eagle Medium (DMEM) without Fetal Bovine Serum (FBS), was formed with the contact angle of 146° meanwhile this angle in lipid contained DMEM solution (by addition of FBS 10%) was 37° (Fig. 1c). Increasing the lipid concentration of DMEM to 20%, resulted in it's well spreading with the contact angle of 25° (Fig. 1d). Other mostly used biocompatible nanostructures such as zinc oxide nanowires (ZnO-NWs) and Graphene sheets were also candidates for such electrodes (Zandi et al., 2019b). Results of wettability tests (discussed in supplementary) showed that graphene sheets (Fig. S1) exhibited super hydrophilic behavior. So, they were rolled out in our investigations. Although ZnO-NWs showed hydrophobic surface (Fig. S2), their conductivity was at least one order of magnitude lower than MWCNTs (Fig. S2) (Chaudhary et al., 2018). Hence, the EIS lipidomics by the CNT decorated electrodes has been investigated.

### 2.2. EIS of cellular secretions

EIS of cellular secretion was carried out on the media of normal (MCF-10A), low grade cancerous (MCF-7), and high grade malignant (MDA-MB-231 & MDA-MB-468) breast cell lines cultured with similar concentration ($3 \times 10^5$ #/well with total volume of 1ml) and vital cycles (analyzed by ANXV/PI method (Fig. 1e & f)). Moreover, between 85 and 90% of the cells from each phenotype were in live cycles meanwhile just less than 8% were in necrosis (Fig. 1f).

Secretions (with the volume of 200 µl) were individually mixed by 0.25ml of 5mM potassium ferricyanide ($K_3Fe(CN)_6$) as background solution before electrical scanning. EIS was recorded in the frequencies ranged between 0.01 to $10^5$ Hz and voltage of 10mv. Fig. 2.a presented the EIS results of cellular secretions. The diameter of semicircular curves, as an indication of charge transfer resistance ($R_{CT}$), is related to current blocking ability of lipid contents of the solution ("Impedance Spectroscopy and Experimental Setup," 2016). $R_{CT}$ was observably greater in secretomes of malignant cells (MDA-MB-231& 468) with respect to low grade cancerous (MCF-7) and normal cells (MCF-10A). To better clarify the key role of lipids in EIS responses of the secretions, the lipid content of culture media from each cell line was individually extracted and redeposited as a semi-solid hydrophobic layer through a known process mentioned in Method section. In summary, the supernatants of the cell lines were collected and their lipids were extracted by the protocols based on extracting hydrophobic structures (chloroform incubation and vacuum drying). So, proteins (as completely hydrophilic macromolecules or structures with one hydrophilic head) wouldn't be captured by this protocol. Then the extracted lipids (Fig. S4) were individually mixed by 0.25ml of $K_3Fe(CN)_6$ and the formed solution was tested by the sensor. Results, presented in Fig. 2.b, showed that the EIS of lipid parts of the secretions exhibited similar responses to that recorded from primary secretion before removing their lipids (Fig. 2.a vs. 2.b). The effect of non-secreted lipids such as FBS (existed in DMEM standard culture media) was excluded in EIS measurements. This was conducted by extracting, weighting and EIS measuring the FBS content of standard media solution (DMEM + 10% FBS) to be considered in our analyses (Fig. 2h).

The lipid free parts of the secretions in all phenotypes of breast cell lines (MCF10A to MDA-MB468) showed similar EIS responses to each other which excluded the role of non-lipidic parts of media (such as proteins or mRNAs) in the response (Fig. 2c). The comparative EIS responses of the whole, lipid parts and lipid free parts of the secretions showed that the charge transfer resistance ($R_{CT}$) of the whole secretion was significantly higher than lipid free part of the secretion with direct dependency to the cancerous state of the cell line while the solution resistance ($R_S$) of the secretion didn't change after removing their lipids (Fig. 2d-f). On the other hand, $R_{CT}$ of lipid part of the secretion was exactly similar to this value in whole secretion (before lipid extraction) for all cell lines. The electrical results were quantitatively tabled in Fig. 2g & h.

When a biological solution is stimulated by AC voltage, macromolecules with dielectric behavior (such as lipids in secretome) play the key role in electrical characteristics of the sample (Hosseini et al., 2016)' (Abdolahad et al., 2014). About one order of magnitude increase could be observed in the EIS response ($R_{CT}$)of lipid contained secretions of malignant breast cells with respect to their lipid free responses while this difference is much lower in the secretome of normal breast cells due to secreting very low concentration of lipids (Fig. S4).

Similar distinguished EIS responses were observed between the secreted media of cancerous and normal of kidney (ACHN vs. HEK 293) (Fig. 3a) as well as primary and progressive grades of ovary cancer (A 2780 vs. OVCAR-3) (Fig. 3b) cell lines all of which were cultured with same parameters as done for breast cell lines. A comparative EIS diagram (Fig. 3c) recorded from the secretomes of breast, kidney, ovary, prostate (PC-3) and stomach (KATO III) cancer cells showed that prostate cancer cells might secret higher concentration of lipids while ovary, stomach and kidney cancer cells secret lower concentration of lipids in comparison with malignant breast cells. This is in correlation with previous reports about the comparative concentration and structures of lipids secreted from prostate and breast cancer cells (Deep and

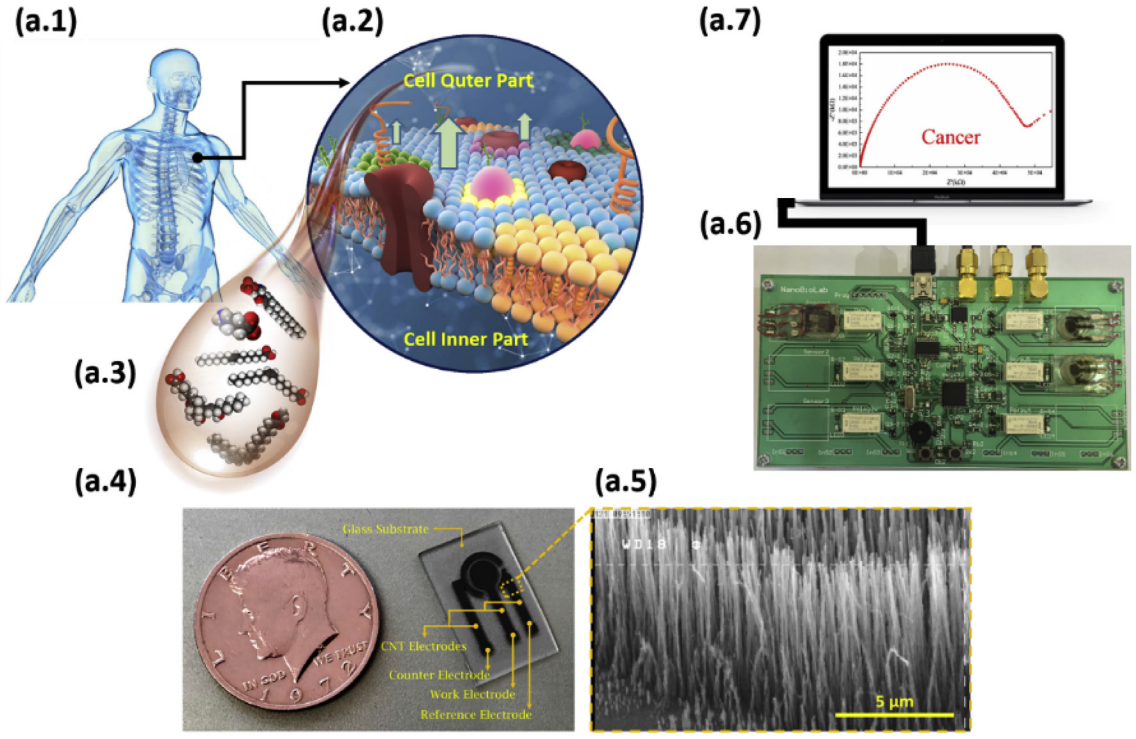


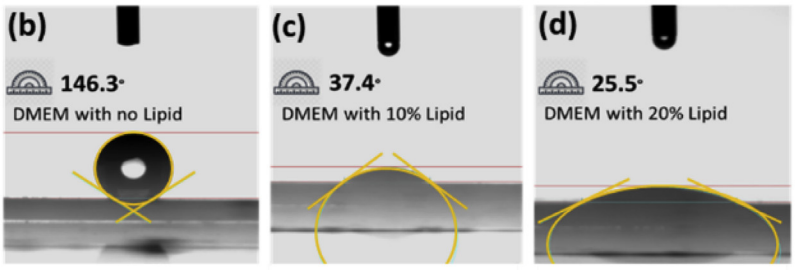


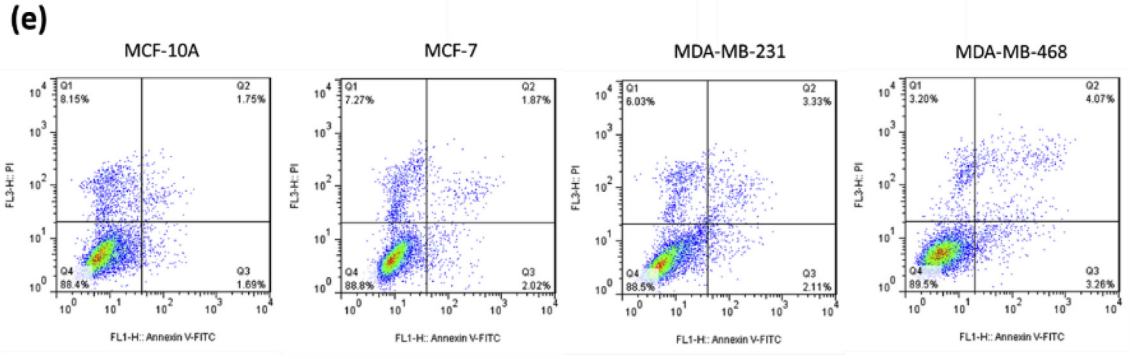


(f)

| Cell Line | MCF-10A (%) | MCF-7 (%) | MDA-MB-231 (%) | MDA-MB-468 (%) |
|---|---|---|---|---|
| Live Cell | 88.4 ± 2.1 | 88.8 ± 2.2 | 88.5 ± 1.8 | 89.5 ± 1.0 |
| Early-Apoptosis | 1.69 ± 0.3 | 2.02 ± 0.23 | 2.11 ± 0.34 | 3.26 ± 0.25 |
| Late-Apoptosis | 1.75 ±0.28 | 1.87 ± 0.09 | 3.33 ± 0.36 | 4.07 ± 0.41 |
| Necrosis | 8.15 ± 0.41 | 7.27 ± 0.39 | 6.03 ± 0.67 | 3.20 ± 0.88 |
| Count | 294559 ± 5514 | 295840 ± 6177 | 295912 ± 5106 | 296947 ± 4991 |

*(caption on next page)*

**Fig. 1.** a) Operational schematic of cancer diagnosis by secretion sensing using EIS. The secreted droplets from the cells, which contain various phenotypic correlated lipid molecules, would be measured by CNT covered EIS device. Presence of cancer cells in the tumor micro-environment is correlated with the indicated intensity of EIS peak. Contact angle measurement of MWCNT surface, revealed the super hydrophobic surface of this structure as the droplet forming angle was 146°, 37° and 25° for b) lipid free DMEM, c) DMEM contain 10% lipid (FBS) and d) DMEM contain 20% lipid respectively. e, f) ANXV/PI analyses of breast cell lines which their secretion had been used for lipid analysis. The concentration of the cells before removing of the secretion were similar ($2.9 \times 10^5$ #/well). It is observable from the table of panel f that all of the cells showed similar vital cycles when their secretions were removed.

Schlaepfer, 2016)' (Beloribi-Djefaflia et al., 2016)' (Tirinato et al., 2017).

### 2.3. Molecular analysis of lipid content in the cellular secretion

Liquid chromatography-mass spectrometry (LC-MS) analysis was conducted on cellular secretions to compare the lipid secreted from different phenotypes of breast cell lines. Extracted lipids (Fig. S4) from each type of cells' media were analyzed by LC-MS (See Methods). A detailed discussion about excluding the probable presence of proteins in extracted lipids from cells' media was presented in supplementary. As presented in Table 1, total molar masses of secreted lipids from the cells were in great correlations with their invasive grades. Total abundance counts of environmental lipids secreted from MDA-MB-468, MDA-MB-231, MCF-7 and MCF-10A cell lines in to the media were 195130, 75394, 56995 and 38385 respectively. This shows the direct relation between increase in lipid content of the media and increased EIS responses (quantified by $R_{CT}$) of cells' secretomes. Moreover, the types of the lipids in the secretion of each cell line exhibited a meaning full match with its phenotypic functions (Table 1). The detected lipids with the mass to charge (m/z) of about 248, the main component in the secretions of all breast cell lines, is attributed to saturated fatty acids (Peck et al., 2016). The counts of these lipids were much further in malignant phenotypes (Table 1). It is indicated that presence of such fatty acid in tumor micro-environment, facilitates tumor expansion (Baenke et al., 2013). The lipids with the m/z of 481, 671 and 673 are related to the exogenous lipids found in tumor micro-environments named lysophosphatic acids (LPA) and phosphatic acids (PA)(Triebl et al., 2014). Ratios of such lipids were greatly further in the secretion of malignant breast cells (MDA-MB-468 and MDA-MB-231, Table 1). It is in correlation with the reports on over secretion of LPA and PA by cancer tumors with respect to normal lesions [24].

Moreover it has been reported that the lipid droplets secreted from cancer cells, contain variable ratios of cholesteryl esters (CEs: m/z of 370) and triglycerides (TAGs: m/z of 507, 515, 520 and 530) with saturated or unsaturated chains (Pol et al., 2014)' (Brasaemle, 2007). Significant amounts of CE and TAGs were traced in the secretions of malignant breast cells (Table 1). Prostaglandins (PGs: m/z of 384 & 394) as a group of lipids with crucial role in proliferation of breast cancer cells (Beloribi-djefa et al., 2016)' (Wang and Dubois, 2006) were found with meaning fully higher levels in high grades of breast cancer cells (Table 1). There were sufficient evidences which revealed that overproduction of the mentioned exogenous lipids is critical for survival of cancer cells as far as overexpression of a central lipogenic enzyme, named fatty acid synthase (FASN), is strongly correlated with cancer progression (Ackerman and Simon, 2014b).

MCF-10A cells (normal breast cell), secreted some additional different types of lipid macromolecules as traced by LC-MS. Nonadecanoic acid (NA: m/z of 187), Phosphatidylethanolamine (PE: m/z of 297) and Sodiated fatty acid (SFA: m/z of 307) contained half of the secreted lipids from normal breast cells. It is known that the mentioned lipids play key role in natural metabolism of normal cells (Tulloch, 1985)' (Tosch et al., 2006)' (Hsu et al., 2014)' (Hsu and Turk, 2010). Our investigations show that both the total counts (specially with further m/z) and $R_{CT}$ of lipids secreted by breast malignant cells were higher than benign types. Lipid abundance of MDA-MB-468, MDA-MB-231, MCF-7 and MCF-10A were about 195000, 75000, 57000 and 38000 respectively. Also the recorded $R_{CT}$ from their secreted lipids by our CNT-EIS system were 39.9, 15.5, 3.9 and 1.3 kΩ respectively. Results were achieved by 5 times repeating the test (STD: ± 5%). The suggested mechanism behind such distinct results between normal and cancer secretomes is related to the increased charge transfer resistance of the solutions contain higher concentration of lipidic macromolecules (cancer samples). In this regard the CNT electrodes greatly transfer all of the frequency dependent stimulating currents to the media and record the transmitted current from the solution depend on lipidic component of the solution ($R_{CT}$ in EIS responses) which is in great correlation with cancerous phenotype of the samples. Lipids not only would extensively attach to the hydrophobic surface of MWCNT electrodes but also their dielectric ability would increase impedance recorded by the electrodes which resulted in enhanced $R_{CT}$ of EIS responses in secretomes of cancer samples.

### 2.4. EIS based lipidomics of live tissues

To apply the electrical lipdomics in cancer diagnosis in real clinical samples, firstly we used from artificial spheroid tumors (prepared from MDA-MB-231cancer cell lines; Fig. 4a).

In this regard, the growth media of tumoral spheroids prepared from MDA-MB-231 breast cancer cell lines (see Methods) was removed and its lipid contents were extracted (Methods). Florescent images showed the well proliferative live states of the spheroids (Fig. 4.a, DAPI: blue) with extended filopodia (Fig. 4.a, actin: green) and dense microtubules (Fig. 4.a, tubulin: red). EIS responses of extracted lipids were measured similar to that was done for 2D cultured MDA-MB-231 cell lines. After comparing the results, it was observed that the $R_{CT}$ of MDA-MB-231 cells' media in spheroid formation was higher than that in 2D culture media (Fig. 4b). Also, the weight of the lipids extracted from spheroids' media was more than that extracted from 2D culture (Fig. 4c).

In next step, the tests were conducted on tumors of mice models. Ten BALB/C female mice (between 5 and 6 weeks) were tumorized by 4T1 (highly wild grade) and MC4L2 (low grade) mouse type breast cancer cells in two individual cohorts (5 mice in each group). The 4T1 and MC4L2 tumors were dissected when their sizes reached to about 60 and 30 $mm^3$ (due to the higher growth rate of 4T1) respectively. Each tumor was immediately cut in 3 spices and hold in spongy foam to absorb all of the peripheral liquids from the tumor environment. The foams were then immersed (soaking and shaking) in standard culture media (without FBS) and after 5 min, the media was processed under lipid extraction procedure (as described above).

Fig. 4.d presented the EIS responses of the lipids extracted from the media solutions of 4T1 and MC4L2 tumors in comparison with the lipids extracted from the 2D culture media of those tumor cell lines. The concentration of the cell lines in first day of culturing was similar to the cells injected to the mice in first day of investigation. Two distinct results could be observed from the EIS plots. First, the $R_{CT}$ (Fig. 4d) and weight (Fig. 4e) of the lipids extracted from 4T1 tumors were further than that in MC4L2 phenotypes which completely corroborates the direct relation between progressed grade of cancer cell line and increased EIS responses of their secretomes. Second, the weight of lipids extracted from the spheroid enviroment were further than that extracted from the 2D culture media (Fig. 4e). These results supported the feasibility of using patients' tumor samples for electrical lipidomic investigations.

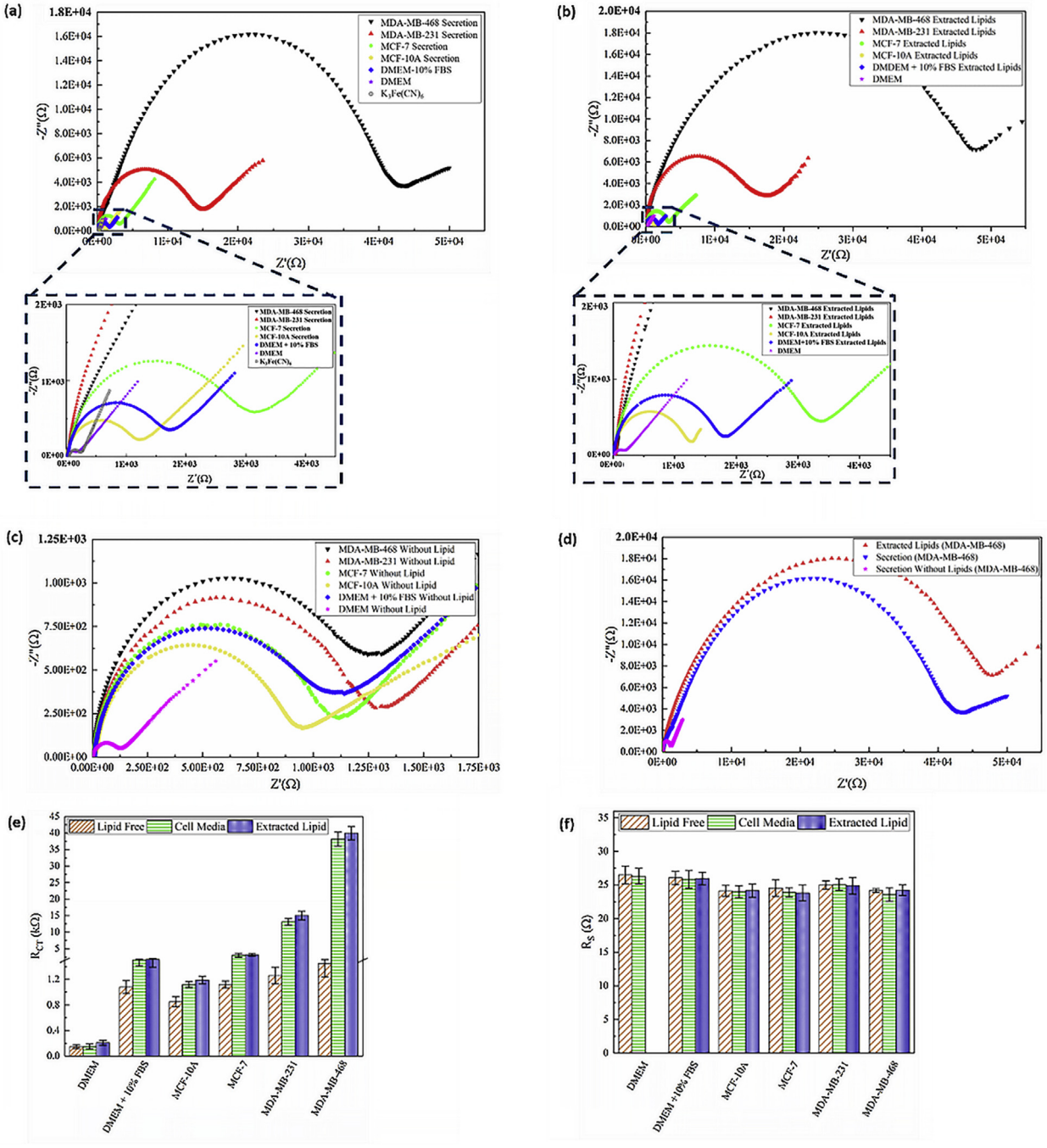


(g)

| Sample | $R_{CT}$, Lipid Free (kΩ) | $R_{CT}$, Cell Media (kΩ) | $R_{CT}$, Extracted Lipid (kΩ) |
|---|---|---|---|
| DMEM | 0.14 ± 0.01 | 0.15 ± 0.01 | 0.21 ± 0.01 |
| DMEM + 10% FBS | 1.08 ± 0.01 | 1.62 ± 0.01 | 1.73 ± 0.01 |
| MCF-10A | 0.85 ± 0.01 | 1.12 ± 0.01 | 1.19 ± 0.01 |
| MCF-7 | 1.12 ± 0.01 | 2.98 ± 0.01 | 3.12 ± 0.01 |
| MDA-MB-231 | 1.26 ± 0.01 | 13.14 ± 0.01 | 15.04 ± 0.01 |
| MDA-MB-468 | 1.45 ± 0.01 | 38.16 ± 0.01 | 39.93 ± 0.01 |

| Sample | $R_S$, Lipid Free (Ω) | $R_S$, Cell Media (Ω) | $R_S$, Extracted Lipid (Ω) |
|---|---|---|---|
| DMEM | 26.5 ± 0.1 | 26.3 ± 0.1 | 0 |
| DMEM + 10% FBS | 26.1 ± 0.1 | 25.8 ± 0.1 | 26.0 ± 0.1 |
| MCF-10A | 24.2 ± 0.1 | 24.1 ± 0.1 | 24.5 ± 0.1 |
| MCF-7 | 24.6 ± 0.1 | 24.0 ± 0.1 | 23.9 ± 0.1 |
| MDA-MB-231 | 25.2 ± 0.1 | 25.3 ± 0.1 | 25.1 ± 0.1 |
| MDA-MB-468 | 24.2 ± 0.1 | 23.7 ± 0.1 | 24.4 ± 0.1 |

(h)

| Sample (10% FBS) | Extracted Lipid Weight ± 0.0001 gr | Sample (0% FBS) | Extracted Lipid Weight ± 0.0001 gr |
|---|---|---|---|
| MDA-MB-468 | 0.2917 | MDA-MB-468 | 0.0401 |
| MDA-MB-231 | 0.1306 | MDA-MB-231 | 0.0110 |
| MCF-7 | 0.0615 | MCF-7 | 0.0021 |
| MCF-10A | 0.0403 | MCF-10A | 0.0005 |
| DMEM | 0.0550 | DMEM | 0.000 |

(caption on next page)

**Fig. 2.** EIS spectroscopy of a) the whole secretion, b) extracted lipid parts and c) lipid free parts of the secretion obtained from the different phenotypes of breast cell lines ranged from normal to metastatic cancer. d) comparative EIS spectra of the secretion of MDA-MB-468 cells in whole secretion, lipid part and lipid free parts. Whole secretion and lipid free parts exhibited similar responses. EIS responses was significantly decreased in lipid free part. e) comparative plots from the charge transfer resistance ($R_{CT}$) between whole secretion, extracted lipid and lipid free parts of the secretion. $R_{CT}$ in the total secretion of cancer cells is more than normal ones meanwhile the lipid free parts of all secretions exhibit similar $R_{CT}$. f) comparative plots of the solution resistance ($R_S$) between whole secretion and lipid free parts of the secretion which presented similar values in all of the breast cell lines. g) values of $R_{CT}$ and $R_S$ recorded from the EIS responses of breast cells' secretion in whole media, lipid part and lipid free part states as quantitative responses of EIS lipidomics system. h) measured weights of extracted lipid parts from different breast cell lines. **Note**: all of the tests were carried out in the mixation of 0.25ml $K_3Fe(CN)_6$. Results derived from 5 repeats of the tests with STD: ± 5%.

### 2.5. EIS based lipid analysis of clinical biopsied breast samples

To evaluate the ability of the lipidomic EIS in tracing the probability of cancer involvement in clinical samples, the peripheral media fluid of the samples resected by core needle biopsy (CNB) with similar sizes from more than 100 patients, suspicious to breast cancer, were recorded (See Methods). The secretions of biopsied samples were collected by spongy foam and the lipids of secretion were extracted and mixed by 0.25ml of $K_3Fe(CN)_6$ through the same protocol described for cell lines. In this regard, the same volume (200 µl) of lipid solutions from each patient's sample were dropped on the surface of the sensor for EIS recording. The reference data for scoring a sample as cancerous (positive) or normal (benign) lesion was standard hematoxylin and eosin (H&E) assay reported by the pathologists. As presented in Fig. 5, a matched range between the $R_{CT}$ of the lipid secretions and pathological diagnosis of the samples was observed with significantly distinguished border. Lipid content in secretion of cancerous samples exhibited one order of magnitude further $R_{CT}$ than normal samples ($10^4$ vs. $10^3$ Ω). The cancer (e.g. Patient #7; Fig. 5b) and normal (e.g. Patient #31; Fig. 5c) secretomes with nearest $R_{CT}$ were of 14.8 kΩ (patient #7) and 7.91 kΩ (patient #31) respectively. This show the promising classification of EIS lipidomics in tissue free diagnosis.

Similar to that done for cell lines, we presented the whole secretion, lipid parts and lipid free parts of EIS responses from cancerous patients (e.g. Fig. 5.d: patient #5 & 5.e: patient #15). It could be also adequate that the lipid part of secretome has the key role in EIS responses and diagnostic scoring of the patients' samples.

Table 2 presented the comparative values between EIS and histopathological results of the biopsied samples, prepared with similar sizes. The $R_{CT}$ in the secretion of normally diagnosed samples was less than 8 kΩ (green column) meanwhile this value was more than 14 kΩ in cancerous samples (red column). Secretion of normal samples exhibited lower $R_{CT}$, due to the rare concentration of lipid content, with meaningful margins (~6 kΩ) from neoplastic samples. After comparison with pathological results of the tissues, 8 of the samples were falsely diagnosed as cancer lesions by EIS lipidomics (false positive, Fig. 6.a.1). Also 3 of the neoplastic samples were falsely missed by EIS lipidomic system (false negative, Fig. 6.b.1). More evaluations on the false positives showed considerable amount of fibrofatty lesions existed in the biopsied samples. H&E images of the neoplastic samples, had been falsely scored negative by EIS, showed small focis of ductal carcinoma in-situ (DCIS) or invasive ductal carcinoma (IDC) which might not include sufficient lipids in their secretion to be detectable by EIS lipidomic system (Fig. 5.a.2 & b.2).

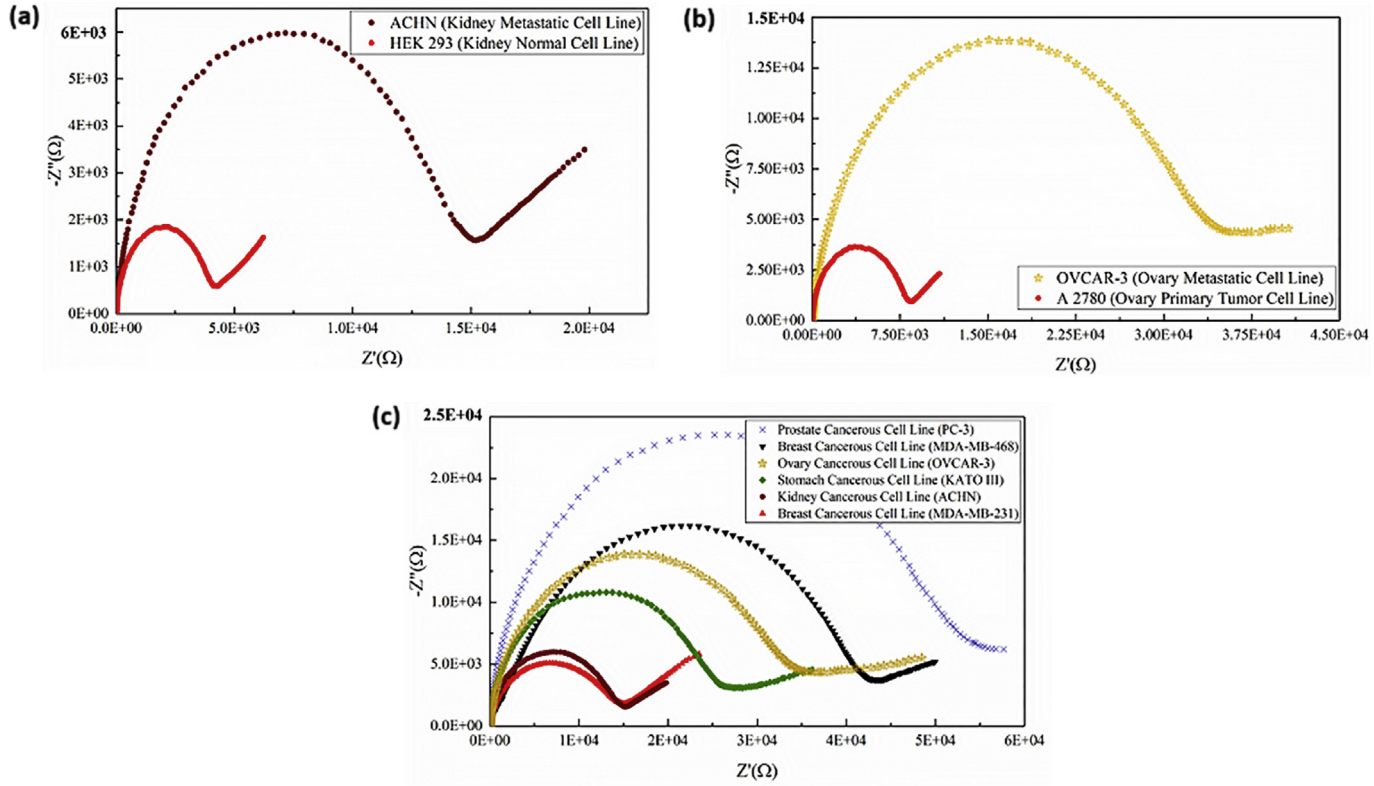


**Fig. 3.** EIS responses of the secreted lipids between normal and cancerous phenotypes were compared in a) kidney as well as primary and progressive grades of cancerous (HEK 293 vs. ACHN). b) Ovary (A 2780 vs. OVCAR-3) cell lines. Similar results to that achieved in breast cell lines were also observed here. c) Comparative EIS spectroscopy of the secreted lipids extracted from cancerous Breast (MDA-MB-468 & MDA-MB-231), prostate (PC-3), ovary (OVCAR-3), stomach (KATO III) and kidney (ACHN) cell lines. **Note:** All of the tests were carried out in the mixation of 0.25ml $K_3Fe(CN)_6$. Results derived from 5 repeats of the tests with STD: ± 5%.

**Table 1**
Individual abundant analysis of lipid contents (based on their molar mass) in the secretion of the breast cell lines ranged from normal to malignant experimented by LC-MS.

| | Abundance | | | | | | Lipid Type |
|---|---|---|---|---|---|---|---|
| Cell type | DMEM + 10%FBS | MDA-MB-468 | MDA-MB-231 | MCF-7 | MCF-10A | DMEM | |
| Lipid Molar mass in secretion (m/z) | | | | | | | |
| 187 | – | – | – | – | 1578 | – | NA |
| 248 | 4029 | 73898 | 20360 | 14000 | 13402 | – | Fatty Acid |
| 267 | – | – | – | – | 1775 | – | |
| 297 | – | – | – | – | 12463 | – | PE |
| 307 | – | – | – | – | 2600 | – | SFA |
| 370 | – | 9097 | 6692 | 5504 | 1559 | – | CE |
| 384 | – | 23580 | 2460 | – | – | – | PG |
| 394 | – | 9948 | 21848 | 13299 | – | – | |
| 481 | 41610 | 14960 | 2794 | – | – | – | LPA&PA |
| 507 | – | – | 6093 | 5299 | | | TAG |
| 515 | 5152 | 6670 | 2529 | – | – | – | |
| 520 | – | 27605 | – | – | – | – | |
| 530 | – | 11061 | 9278 | 2698 | 2186 | – | |
| 647 | 19556 | 6706 | – | 4152 | 2822 | – | LPA&PA |
| 671 | – | 11605 | – | – | – | – | |
| 673 | 18137 | – | 3340 | 12043 | – | – | |
| *Total* | *51,035* | *195,130* | *75,394* | *56,995* | 38,385 | – | |

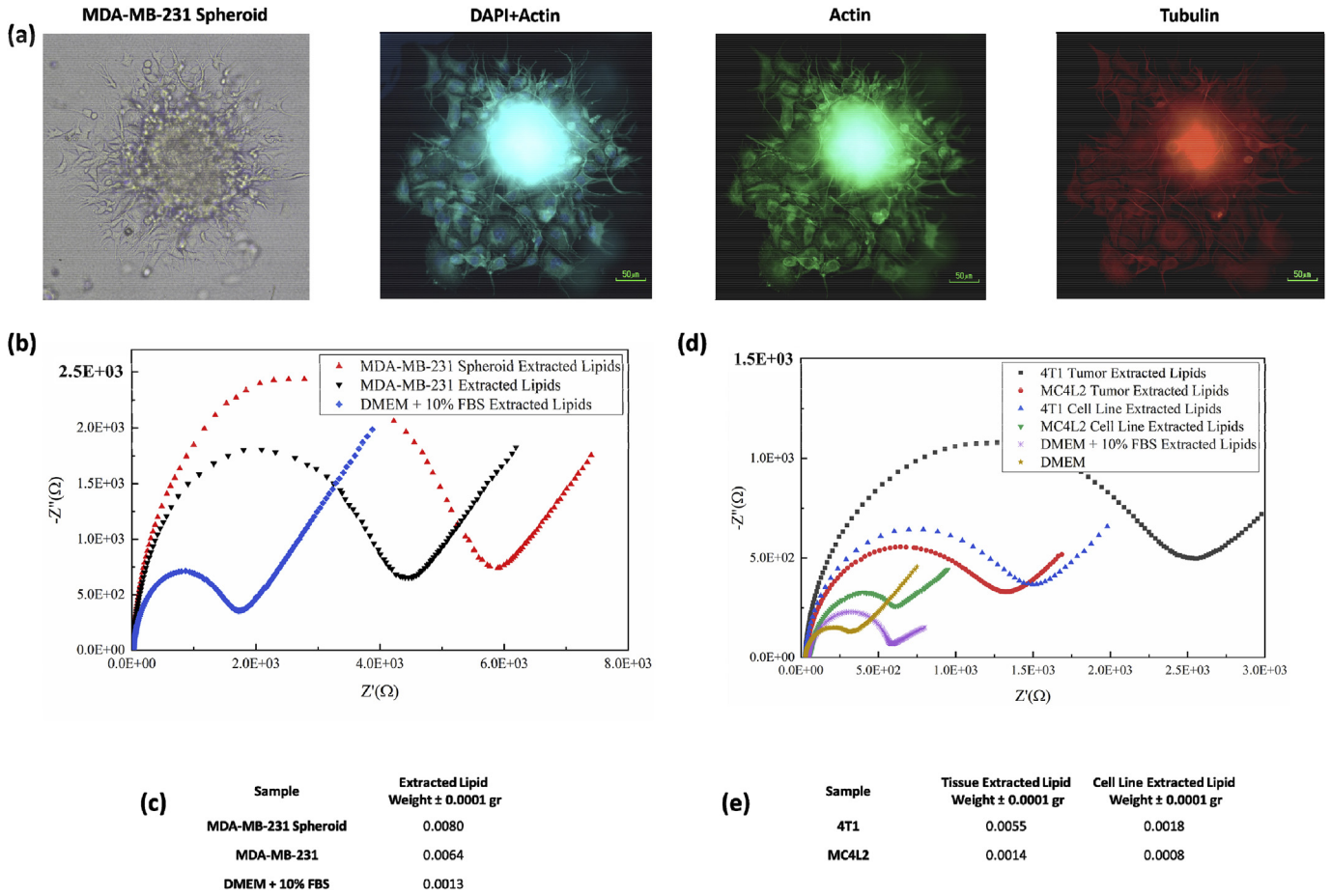


(c)

| Sample | Extracted Lipid Weight ± 0.0001 gr |
|---|---|
| MDA-MB-231 Spheroid | 0.0080 |
| MDA-MB-231 | 0.0064 |
| DMEM + 10% FBS | 0.0013 |

(e)

| Sample | Tissue Extracted Lipid Weight ± 0.0001 gr | Cell Line Extracted Lipid Weight ± 0.0001 gr |
|---|---|---|
| 4T1 | 0.0055 | 0.0018 |
| MC4L2 | 0.0014 | 0.0008 |

**Fig. 4.** a) optical microscopy, DAPI (blue), actin (green) and tubulin (red) florescent images of MDA-MB-231 cells formed in spheroid shape. b) EIS responses of the secreted lipids between spheroid and 2D cultured states of MDA-MB-231 cell lines were compared. c) the table of the lipid weight secreted from MDA-MB-231 cells in spheroid and 2D cultured states. d) comparative EIS responses of the secreted lipids from mice 4T1 and MCFL2 breast cell lines between in-vivo tumor formed and in-vitro cell cultured states. e) the weight of lipid extracted from the mentioned mice samples. (For interpretation of the references to color in this figure legend, the reader is referred to the Web version of this article.)

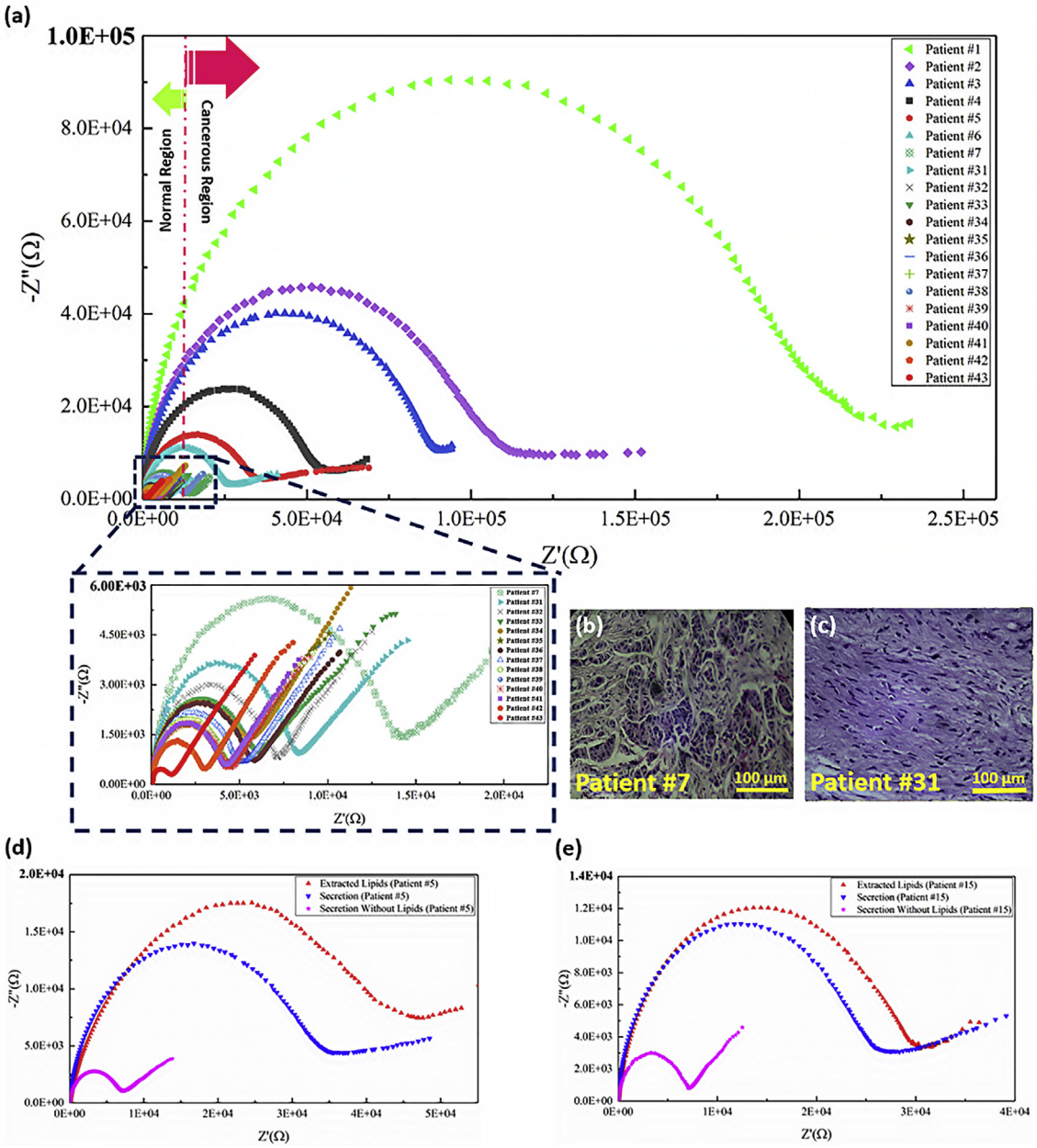


**Fig. 5.** a) EIS spectroscopy of the lipid content of the secretions collected from the breast biopsied tissues of 20 patients suspicious to breast cancer. The size and volume of the samples were similar. The derived lipids were individually mixed by 0.25 ml of $K_3Fe(CN)_6$ and then were casted on the sensors. A distinguishable border could be observed between normal and cancer tissues which were confirmed by parallel H&E pathological method presented in panels b and c for two cancerous and normal samples as examples respectively. Cancer cells show larger nucleus with increased nucleus/cytoplasm ratio and hyper chromic stain. The nest of tumor cells with increased nucleus/cytoplasm ratio and hyperchromic nucleus shape with distinguishable shapes in stroma confirmed the neoplastic function of the cells in biopsied sample. EIS responses of the secretion from two cancerous patients; d) patient #5 and e) patient #15 revealed the meaningful distance between the impedance spikes of lipid free part and whole of the secretion (all mixed by $K_3Fe(CN)_6$ before recording) while lipid part of the secretion exhibited great similar EIS behavior to the primary secretion.

## 3. Conclusion

In summary, we developed electrochemical lipidomics based on EIS of the tissue secretions to diagnose cancer samples due to the concentration of their lipid contents. Applying MWCNT arrays as conductive nanostructures with super hydrophobic surface, enhanced the interactive area between secreted lipids and the electrodes to improve the precision of the $R_{CT}$ recorded from the secretome. The EIS of lipids extracted from the media solution of spheroid cell lines, mice model breast cancer tumors and finally breast CNBs of more than 100 human samples showed distinguished response profile between normal and cancer cells. A sharp quantitative boundary of $R_{CT}$ between normal ($< 8$ KΩ) and cancer ($> 13$ kΩ) was recorded by the system on human biopsy secretion. By considering both false positives and negatives, EIS lipidomics showed about 90% precision in cell free (secretion based) diagnosis of the neoplastic nature of breast biopsied samples without inducing any disruption on conventional pathological procedures. Simple use, low volume of required analyte (a droplet of secretion) and fast analysis without inducing any perturbation to the main biopsied sample are the distinct advantages of EIS lipidomics in new era of cancer diagnosis.

**Table 2**
EIS of secretion, H&E, tissue size and $R_{CT}$ results of breast biopsied samples (by CNB) prepared from 100 patients suspicious to breast cancer. Each test repeated for 5 times with STD: ± 5%.

| Patient ID | EIS Secretion Sensor | Pathological Diagnosis | Size Sample ± 0.001 $cm^3$ | $R_{CT}$ (KΩ) |
|---|---|---|---|---|
| 1 | + | + | 1.1×0.9×0.3 | 193 |
| 2 | + | + | 2.9×2.1×1.0 | 101.8 |
| 3 | + | + | 0.9×0.7×0.2 | 82.5 |
| 4 | + | + | 1.4×1.3×0.8 | 51.8 |
| 5 | + | + | 1.0×0.9×0.4 | 33.68 |
| 6 | + | + | 0.8×0.8×0.7 | 24.86 |
| 7 | + | + | 1.4×1.1×0.5 | 14.80 |
| 8 | + | + | 1.0×1.1×0.3 | 27.50 |
| 9 | + | + | 1.9×0.9×1.0 | 94.87 |
| 10 | + | + | 1.0×0.5×0.5 | 46.05 |
| 11 | + | + | 1.8×1.3×0.9 | 46.05 |
| 12 | + | + | 1.0×1.0×0.2 | 63.39 |
| 13 | + | + | 2.1×1.4×0.4 | 114.1 |
| 14 | + | + | 1.0×0.7×0.6 | 71.16 |
| 15 | + | + | 1.1×1.0×0.3 | 75.02 |
| 16 | + | + | 1.0×1.0×0.4 | 14.26 |
| 17 | + | + | 1.7×1.2×0.2 | 19.45 |
| 18 | + | + | 1.5×1.0×0.5 | 15.94 |
| 19 | + | + | 1.6×1.2×0.4 | 19.95 |
| 20 | + | + | 1.2×1.2×1.0 | 27.63 |
| 21 | + | + | 1.7×1.6×0.5 | 23.03 |
| 22 | + | + | 1.8×0.8×0.8 | 15.85 |
| 23 | + | + | 2.2×1.9×0.4 | 16.64 |
| 24 | + | + | 1.3×0.9×0.3 | 37.20 |
| 25 | + | + | 1.6×1.0×0.5 | 39.93 |
| 26 | + | + | 0.9×0.9×0.7 | 16.87 |
| 27 | + | + | 1.0×1.0×0.5 | 15.04 |
| 28 | + | + | 1.4×1.1×0.2 | 14.49 |
| 29 | + | + | 1.6×1.4×0.6 | 14.07 |
| 30 | + | + | 1.8×0.7×0.7 | 19.97 |
| 31 | – | – | 2.0×2.0×1.0 | 7.91 |
| 32 | – | – | 0.9×0.7×0.2 | 7.88 |
| 33 | – | – | 1.1×0.8×0.5 | 6.55 |
| 34 | – | – | 1.2×1.2×0.4 | 5.65 |
| 35 | – | – | 1.0×0.9×0.9 | 5.38 |
| 36 | – | – | 1.5×1.2×0.8 | 4.14 |
| 37 | – | – | 1.9×1.7×0.6 | 3.94 |
| 38 | – | – | 1.5×0.9×0.9 | 3.90 |
| 39 | – | – | 2.1×1.3×1.1 | 2.78 |
| 40 | – | – | 1.6×1.4×0.3 | 5.08 |
| 41 | – | – | 1.3×0.9×0.8 | 4.79 |
| 42 | – | – | 2.3×2.2×1.0 | 4.12 |
| 43 | – | – | 1.8×1.5×1.1 | 4.08 |
| 44 | – | – | 1.1×1.0×1.0 | 1.10 |
| 45 | – | – | 1.2×1.0×0.5 | 2.30 |
| 46 | – | – | 1.9×1.2×1.0 | 2.87 |
| 47 | – | – | 1.8×1.7×1.0 | 1.17 |
| 48 | – | – | 1.5×1.4×0.6 | 5.88 |
| 49 | – | – | 2.9×1.8×0.5 | 2.37 |
| 50 | – | – | 3.0×2.2×1.0 | 3.78 |
| 51 | – | – | 1.9×1.6×0.9 | 7.25 |
| 52 | – | – | 0.8×0.8×0.8 | 0.79 |
| 53 | – | – | 1.7×1.0×1.0 | 2.25 |
| 54 | – | – | 2.1×2.0×1.5 | 3.12 |
| 55 | – | – | 1.2×1.2×1.0 | 1.67 |
| 56 | – | – | 1.5×1.1×0.2 | 2.81 |
| 57 | – | – | 1.8×1.3×0.4 | 1.81 |
| 58 | – | – | 1.1×1.0×0.3 | 2.63 |
| 59 | – | – | 1.0×0.9×0.9 | 1.30 |
| 60 | – | – | 1.1×0.9×0.8 | 2.69 |
| 61 | – | – | 1.9×1.5×1.0 | 2.34 |
| 62 | – | – | 1.0×1.0×0.9 | 3.38 |
| 63 | – | – | 0.9×0.5×0.5 | 1.75 |
| 64 | – | – | 1.7×1.2×1.0 | 0.76 |
| 65 | – | – | 2.2×0.9×0.6 | 1.80 |
| 66 | – | – | 1.9×1.5×1.5 | 0.61 |
| 67 | – | – | 1.8×1.4×0.4 | 1.75 |
| 68 | – | – | 1.3×1.1×0.8 | 2.67 |
| 69 | – | – | 1.7×0.9×0.8 | 1.59 |
| 70 | – | – | 0.9×0.9×0.9 | 0.94 |
| 71 | – | – | 1.2×1.2×1.0 | 3.12 |
| 72 | – | – | 2.2×2.0×1.5 | 5.10 |
| 73 | – | – | 1.6×1.4×0.7 | 3.76 |
| 74 | – | – | 1.5×1.0×1.0 | 7.76 |
| 75 | – | – | 1.4×0.9×0.5 | 6.70 |
| 76 | – | – | 1.3×1.1×0.6 | 7.69 |
| 77 | – | – | 1.9×1.4×0.6 | 2.83 |
| 78 | – | – | 1.7×1.2×1.0 | 3.87 |
| 79 | – | – | 1.4×0.9×0.9 | 0.73 |
| 80 | – | – | 0.9×0.8×0.3 | 0.79 |
| 81 | – | – | 1.5×1.5×1.0 | 4.06 |
| 82 | – | – | 1.6×1.1×1.1 | 5.50 |
| 83 | – | – | 2.1×1.7×0.9 | 5.10 |
| 84 | – | – | 1.0×0.9×0.2 | 6.05 |
| 85 | – | – | 1.6×1.4×0.7 | 2.53 |
| 86 | – | – | 1.8×1.0×1.0 | 0.79 |
| 87 | – | – | 2.9×0.8×0.8 | 1.43 |
| 88 | – | – | 2.3×1.7×1.3 | 1.33 |
| 89 | – | – | 1.0×0.2×0.2 | 1.24 |
| 90 | – | – | 1.9×1.2×0.5 | 2.59 |
| 91 | – | – | 2.1×0.5×0.2 | 4.69 |
| 92 | – | – | 1.3×1.3×0.8 | 3.43 |
| 93 | – | – | 1.7×1.2×0.5 | 5.10 |
| 94 | – | – | 0.9×0.4×0.2 | 5.09 |
| 95 | – | – | 1.5×1.5×0.4 | 1.80 |
| 96 | – | – | 2.2×1.0×0.9 | 4.61 |
| 97 | – | – | 0.5×0.5×0.5 | 3.21 |
| 98 | – | – | 1.7×0.9×0.3 | 1.65 |
| 99 | – | – | 1.1×1.0×0.2 | 0.97 |
| 100 | – | – | 0.7×0.7×0.3 | 0.98 |

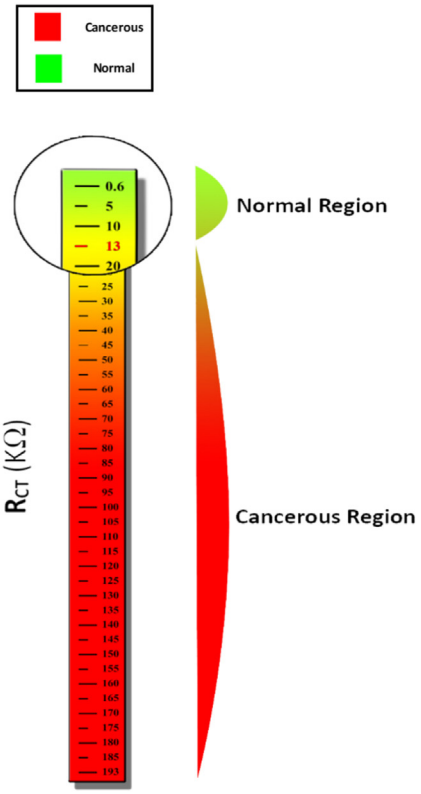


## 4. Materials and methods

### 4.1. Cell culture

Cell lines used in this experiment are MCF-10A, MCF-7, MDA-MB-231 and MDA-MB-468 human breast normal and cancer cell lines, HEK-293 & ACHN human kidney normal and cancer cell lines, A-2780 & OVCAR-3 human ovary primary and progressive grades of cancer cell lines, PC-3 prostate cancer cell line, KATO-III stomach cancer cell line and MC4L2 & 4T1 primary and progressive grades of mice breast cancer cell lines acquired from national cell bank of Iran (Pasteur Institute) and Iranian Biological Resource Center (IBRC). Cell lines (except MCF-10A) were kept in DMEM culture medium (Gibco) complimented with 5% fetal bovine serum (Sigma) and 1% penicillin/streptomycin (Gibco) at 37 °C (5% $CO_2$, 95% filtered air). MCF-10A was maintained in DMEM culture medium supplemented with 5% horse serum (Invitrogen), 100 µg/ml EGF (Peprotech), 1 mg/ml hydrocortisone (Sigma), 1 mg/ml cholera toxin (Sigma), 10 mg/ml insulin (Sigma) and 1% penicillin/streptomycin (Gibco). Manual cell counting method, haemocytometer neubauer, has been used to determine primary populations of the cell lines (Camacho-Fernández et al., 2018).

### 4.2. Lipid extraction from the secretion

Usually cell media (without FBS or BSA) are lipid free. Most basic way to measure lipid content is adding equal volume of 1:2 Chloroform/methanol to your media, let the phase separate and collect the bottom fraction, dry under vacuum to separate a thin-layer of lipid content directly secreted from the cells. This layer might also contain hydrophobic proteins named as lipoproteins which we assumed them in the lipid categories here. To avoid peroxidation of the extracted lipids, during the procedure or later, all solvents should be used peroxide-free. This hydrophobic lipid layer then was dropped on the sensor and extended on it due to super hydrophobicity of CNTs. Then the EIS was recorded from the sample. The sample was also analyzed by mass spectroscopy to evaluate the lipid types that might be found. In the case

(a)

| False Positives | | | | |
|---|---|---|---|---|
| Patient ID | EIS Secretion Sensor | Pathological Diagnosis | Size Sample ± 0.001 cm³ | $R_{CT}$ (kΩ) |
| 101 | + | – | 1.0×1.1×0.9 | 14.25 |
| 102 | + | – | 1.4×1.2×0.5 | 13.91 |
| 103 | + | – | 2.1×0.9×0.8 | 15.44 |
| 104 | + | – | 1.1×1.0×1.0 | 16.10 |
| 105 | + | – | 1.5×1.0×1.0 | 14.79 |

(c)

| False Negatives | | | | |
|---|---|---|---|---|
| Patient ID | EIS Secretion Sensor | Pathological Diagnosis | Size Sample ± 0.001 cm³ | $R_{CT}$ (kΩ) |
| 106 | – | + | 1.3×1.0×1.0 | 5.31 |
| 107 | – | + | 0.9×0.9×0.8 | 2.74 |
| 108 | – | + | 1.9×1.4×0.4 | 6.38 |

(b)

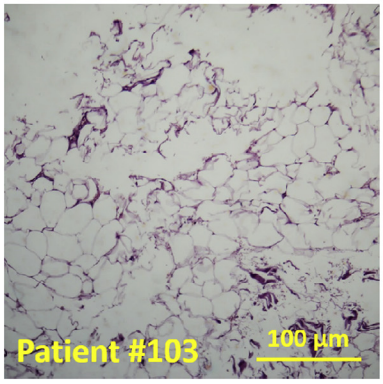


(d)

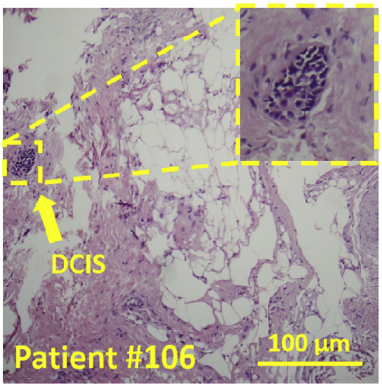


**Fig. 6.** a) false positive, b) an example from H&E image of a sample falsely scored positive by EIS which contains breast fatty tissues, c) false negative results of EIS responses recorded from biopsied breast samples, d) an example from H&E images of a neoplastic samples negatively scored by EIS showed small foci of DCIS (~1%) in the lesions which might not include sufficient lipids in their secretion to be detected by EIS lipidomics.

of tissue sample, similar volume of tissues from normal or cancer phenotypes were prepared through standard protocols of surgery or biopsy and then held on a dry spongy foam to absorb the secreted and peripheral solution of the tissue for about 10 min. Then the foam was held in non-polar chloroform solution for 10 min in a shaker. Then the foam was removed and the methanol was added to secretion containing chloroform sample in the ratio of 1:2 chloroform: methanol. Then the lipid extraction process was carried out as described above.

### 4.3. Electrical measurement

In order to carry out the dielectric spectroscopy on cellular secretion, the lipid extracted from similar concentration of cell lines or similar volume of tissues were mixed by 0.25 ml of potassium ferricyanide ($K_3Fe(CN)_6$) and casted on CNT covered fabricated integrated sensor. The response was recorded using portable electrochemical analyser (IVIUM, Compactstat.h) in three –electrode electrochemical impedance spectroscopy (EIS) mode. The aforementioned electrodes were calibrated using potassium ferricyanide ($K_3Fe(CN)_6$). The EIS was performed at 10 mV AC voltage sweeping the frequency from 100 kHz to 0.01 Hz at 255 points.

### 4.4. Mass spectrometry

Liquid chromatography Mass Spectrometry (LC-MS) was performed using an Agilent LC/MS-6410 Triple Quadruple mass spectrometer interfaced with electrospray ionization (ESI) ion source. In order to diagnose and determine the lipid content, the negative selected ion monitoring (SIM) mode were chosen. Nitrogen at flow rate of 6 L/min was used as drying and nebulizing gas adjusted at 15 psi. The capillary voltage and desolvation temperature were 4.0 kV and 300 °C respectively. MassHunter software used to process the data.

### 4.5. Fabrication of the device

The fabrication process of the device was started by coating the SiO2/glass surface with a thermally grown Ni layer, followed by patterning using standard photolithography. Finally, the sample is placed in a direct-current plasma enhanced chemical vapor deposition (DC-PECVD) reactor to grow vertically aligned multi-walled carbon nanotubes (MWCNTs) on desired places in a manner reported elsewhere (Zandi et al., 2019a). The CNT beam length and diameter range from 8 to 12 µm and 20–75 nm, respectively. Fig. 1a.4 depicts the patterned CNT sensor which the working, counter and reference electrodes has been defined. All three mentioned electrodes made from the grown CNTs. Fig. 1.a.5 shows the SEM image of the device. Highly ordered CNTs have been achieved with desired patterns and geometries. Fig. S6 depicts process flow of the fabricated sensors.

### 4.6. Biopsy sample preparation

#### 4.6.1. Core needle biopsy (CNB)

This process was carried out to prepare live specimen from the tissue suspicious to malignancy. A hollow steel tube was applied to withdraw small cylinders (or cores) of tissue of the targeted region in the breast or sentinel lymph nodes by the interventional radiologist or surgeon. The core needle was put in 3–6 times to detach multiple samples, or cores. The process was done under ultrasonic guidance to put the needle into the right place.

### 4.7. Pathological procedure

Hematoxylin and eosin (H&E) has been used as a popular staining technique in histopathology. Combination of two dyes, hematoxylin and eosin used for illustration of nucleus and cytoplasmic inclusions in clinical specimens. Hematoxylin containing alum (alum acts as mordant) stains the nucleus light blue. Presence of acid would turn it to red

if differentiation was achieved by exposing the tissue to acid solution. Red color within the nucleus (initial soluble color) turns to an insoluble blue color during the bluing step. As the counterstaining, eosin brings pink color to the cytoplasm. The biopsied tissue H&E staining process will be initiated by deparaffinizing the section, flaming the slide on burner, and locating it in the xylene. The treatment would be repeated followed by hydration though reducing the concentration of alcohol baths and water (100, 90, 80, 70%). Staining by hematoxylin for 3–5 min was then done followed by washing in running tap water until sections "blue" for 5 min or less. Next, the differentiation in 1% acid alcohol (1% HCl in 70% alcohol) for 5 min would be carried out. Sequential washing the sample in running tap water and dipping in an alkaline solution (eg., ammonia water) until the sections being blue were the final steps. The sample was then stained in 1% eosin Y for 10 min and washed in tap water for 1–5 min, and then dehydration in increasing concentration of alcohols and clearing in xylene were done.

### 4.8. Spheroid formation procedure

MDA-MB-231 cells were trypsinized and after counting, droplets with volume of 20 μl were deposited on the lid of non-adhesive culture dishes. The dishes were then inverted and incubated (37 °C and 5% CO2) for 2 days. After formation of the desired size of the spheroids, the droplets were collected and added to the collagen matrix (rat tail, Corning). Afterwards, the mixture of collagen and spheroids were transferred into 96 well microplate followed by incubation for 30 min. Finally after gel crosslinking, the cell culture medium was added to each well.

### 4.9. Mice tumorgenicity procedure

Female BALB/C mice, 5–6 weeks old, were purchased from Pasteur Institute of Iran. All the mice were kept in standard condition. MC4L2 and 4T1 cell lines were prepared ($2 \times 10^6/0.2\,ml^{-1}$) and injected in mammary gland of female mice under ketamine and xylazine anesthesia, 50 mg/kg and 10 mg/kg i.p., respectively. Animal studies were performed in accordance with guidelines for the care and use of laboratory animals. The protocol was officially approved by animal ethics committee of Iran. When the tumor size reached to the desired size, the mice were euthanatized and tumors were dissected.

## CRediT authorship contribution statement

**Ashkan Zandi:** Data curation, Formal analysis, Investigation. **Ali Gilani:** Formal analysis, Methodology, Visualization. **Fereshteh Abbasvandi:** Methodology, Validation, Investigation. **Pouyan Katebi:** Formal analysis, Methodology, Visualization. **Saeid Rafizadeh Tafti:** Methodology, Validation, Investigation. **Sepanta Assadi:** Formal analysis, Methodology, Visualization. **Hassan Moghtaderi:** Formal analysis, Methodology, Visualization. **Mohammad Salemizadeh Parizi:** Formal analysis, Methodology, Visualization. **Mohammad Saghafi:** Formal analysis, Methodology, Visualization. **Mohammad Ali Khayamian:** Formal analysis, Methodology, Visualization. **Zahra Davari sh:** Formal analysis, Methodology, Visualization. **Parisa Hoseinpour:** Methodology, Validation, Investigation. **Masoumeh Gity:** Methodology, Validation, Investigation. **Hassan Sanati:** Methodology, Validation, Investigation. **Mohammad Abdolahad:** Conceptualization, Formal analysis, Supervision, Project administration, Writing - original draft, Writing - review & editing.

## Acknowledgements

We thank Dr M. Abdollahi (MD. MPA) for advice on H&E Staining; Dr. M. Faranoush (MD. Professor. Rasul Akram hospital, Department of Oncology) for critical discussion about the cancer metastasis. Finally, we thank professor S. Sarkar, Dr. H. Shakki and Mr. M. Zeighami for their great support on this project (INIC). This work is supported by the Vice Presidency for Science and Technology, Technology Studies Institute (No. TSI-95-33-8-028) and the INSF (No. 35822859). A provisional USA patent on this work was registered by M.A.

## Appendix A. Supplementary data

Supplementary data to this article can be found online at https://doi.org/10.1016/j.bios.2019.111566.

## References

Abdolahad, M., Shashaani, H., Janmaleki, M., 2014. Biosensors and Bioelectronics Silicon nanograss based impedance biosensor for label free detection of rare metastatic cells among primary cancerous colon cells , suitable for more accurate cancer staging. Biosens. Bioelectron. 59, 151–159. https://doi.org/10.1016/j.bios.2014.02.079.

Ackerman, D., Simon, M.C., 2014a. Hypoxia, lipids, and cancer: surviving the harsh tumor microenvironment. Trends Cell Biol. 24, 472–478. https://doi.org/10.1016/j.tcb.2014.06.001.

Ackerman, D., Simon, M.C., 2014b. Hypoxia, lipids, and cancer: surviving the harsh tumor microenvironment. Trends Cell Biol. 24, 472–478. https://doi.org/10.1016/j.tcb.2014.06.001.

Apicella, M., Giannoni, E., Fiore, S., Ferrari, K.J., Fernández-Pérez, D., Isella, C., Granchi, C., Minutolo, F., Sottile, A., Comoglio, P.M., Medico, E., Pietrantonio, F., Volante, M., Pasini, D., Chiarugi, P., Giordano, S., Corso, S., 2018. Increased lactate secretion by cancer cells sustains non-cell-autonomous adaptive resistance to MET and EGFR targeted therapies. Cell Metabol. 28, 848–865. e6. https://doi.org/10.1016/j.cmet.2018.08.006.

Baenke, F., Peck, B., Miess, H., Schulze, A., 2013. Hooked on Fat : the Role of Lipid Synthesis in Cancer Metabolism and Tumour Development, vol. 1363. pp. 1353–1363. https://doi.org/10.1242/dmm.011338.

Beloribi-djefa, S., Vasseur, S., Guillaumond, F., 2016. Lipid metabolic reprogramming in cancer cells. https://doi.org/10.1038/oncsis.2015.49.

Beloribi-Djefaflia, S., Vasseur, S., Guillaumond, F., 2016. Lipid metabolic reprogramming in cancer cells. Oncogenesis 5, e189. https://doi.org/10.1038/oncsis.2015.49.

Binnewies, M., Roberts, E.W., Kersten, K., Chan, V., Fearon, D.F., Merad, M., Coussens, L.M., Gabrilovich, D.I., Ostrand-Rosenberg, S., Hedrick, C.C., Vonderheide, R.H., Pittet, M.J., Jain, R.K., Zou, W., Howcroft, T.K., Woodhouse, E.C., Weinberg, R.A., Krummel, M.F., 2018. Understanding the tumor immune microenvironment (TIME) for effective therapy. Nat. Med. 24, 541–550. https://doi.org/10.1038/s41591-018-0014-x.

Bose, T., Cie, A., Wiechec, E., 2015. Role of ion channels in regulating Ca 2 + homeostasis during the interplay between immune and cancer cells 1–11. https://doi.org/10.1038/cddis.2015.23.

Brasaemle, D.L., 2007. *Thematic review series: adipocyte Biology* . The perilipin family of structural lipid droplet proteins: stabilization of lipid droplets and control of lipolysis. J. Lipid Res. 48, 2547–2559. https://doi.org/10.1194/jlr.R700014-JLR200.

Brügger, B., 2014. Lipidomics: analysis of the lipid composition of cells and subcellular organelles by electrospray ionization mass spectrometry. Annu. Rev. Biochem. 83, 79–98. https://doi.org/10.1146/annurev-biochem-060713-035324.

Camacho-Fernández, C., Hervás, D., Rivas-Sendra, A., Marín, M.P., Seguí-Simarro, J.M., 2018. Comparison of six different methods to calculate cell densities. Plant Methods 14, 1–15. https://doi.org/10.1186/s13007-018-0297-4.

Chaudhary, S., Umar, A., Bhasin, K.K., Baskoutas, S., 2018. Chemical sensing applications of ZnO nanomaterials. Materials 11, 1–38. https://doi.org/10.3390/ma11020287.

Chen, M., Zhang, J., Sampieri, K., Clohessy, J.G., Mendez, L., Gonzalez-Billalabeitia, E., Liu, X.S., Lee, Y.R., Fung, J., Katon, J.M., Menon, A.V., Webster, K.A., Ng, C., Palumbieri, M.D., Diolombi, M.S., Breitkopf, S.B., Teruya-Feldstein, J., Signoretti, S., Bronson, R.T., Asara, J.M., Castillo-Martin, M., Cordon-Cardo, C., Pandolfi, P.P., 2018. An aberrant SREBP-dependent lipogenic program promotes metastatic prostate cancer. Nat. Genet. 50, 206–218. https://doi.org/10.1038/s41588-017-0027-2.

De Palma, M., Biziato, D., Petrova, T.V., 2017. Microenvironmental regulation of tumour angiogenesis. Nat. Rev. Cancer 17, 457–474. https://doi.org/10.1038/nrc.2017.51.

Deep, G., Schlaepfer, I.R., 2016. Aberrant lipid metabolism promotes prostate cancer: role in cell survival under hypoxia and extracellular vesicles biogenesis. Int. J. Mol. Sci. 17. https://doi.org/10.3390/ijms17071061.

Finicle, B.T., Jayashankar, V., Edinger, A.L., 2018. Nutrient scavenging in cancer. Nat. Rev. Cancer 18, 619–633. https://doi.org/10.1038/s41568-018-0048-x.

Gramse, G., Dols-Perez, A., Edwards, M.A., Fumagalli, L., Gomila, G., 2013. Nanoscale measurement of the dielectric constant of supported lipid bilayers in aqueous solutions with electrostatic force microscopy. Biophys. J. 104, 1257–1262. https://doi.org/10.1016/j.bpj.2013.02.011.

Hosseini, S.A., Abdolahad, M., Zanganeh, S., Dahmardeh, M., Gharooni, M., Abiri, H., Alikhani, A., Mohajerzadeh, S., Mashinchian, O., 2016. Nanoelectromechanical chip (NELMEC) combination of nanoelectronics and microfluidics to diagnose epithelial and mesenchymal circulating tumor cells from leukocytes. Small 12, 883–891. https://doi.org/10.1002/smll.201502808.

Hsu, F.F., Matthew Kuhlmann, F., Turk, J., Beverley, S.M., 2014. Multiple-stage linear ion-trap with high resolution mass spectrometry towards complete structural characterization of phosphatidylethanolamines containing cyclopropane fatty acyl chain in Leishmania infantum. J. Mass Spectrom. 49, 201–209. https://doi.org/10.1002/jms.3327.

Hsu, F.F., Turk, J., 2010. Electrospray ionization multiple-stage linear ion-trap mass spectrometry for structural elucidation of triacylglycerols: assignment of fatty acyl groups on the glycerol backbone and location of double bonds. J. Am. Soc. Mass Spectrom. 21, 657–669. https://doi.org/10.1016/j.jasms.2010.01.007.

Impedance Spectroscopy and Experimental Setup, 2016. https://doi.org/10.1007/978-3-319-32655-9.

Joshi, H., Maiti, P.K., 2018. Structure and electrical properties of DNA nanotubes embedded in lipid bilayer membranes. Nucleic Acids Res. 46, 2234–2242. https://doi.org/10.1093/nar/gkx1078.

Karagiannis, G.S., Pavlou, M.P., Diamandis, E.P., 2010. Cancer Secretomics Reveal Pathophysiological Pathways in Cancer Molecular Oncology, vol. 4. https://doi.org/10.1016/j.molonc.2010.09.001.

Kurtova, A.V., Xiao, J., Mo, Q., Pazhanisamy, S., Krasnow, R., Lerner, S.P., Chen, F., Roh, T.T., Lay, E., Ho, P.L., Chan, K.S., 2014. Abrogates bladder cancer chemoresistance. Nature 517, 209–213. https://doi.org/10.1038/nature14034.

Luo, X., Zhao, X., Cheng, C., Li, N., Liu, Y., Cao, Y., 2018. The implications of signaling lipids in cancer metastasis. Exp. Mol. Med. 50. https://doi.org/10.1038/s12276-018-0150-x.

Me, O., 2013. Unconventional secretion is a major contributor of cancer cell line secretomes * □ laura villarreal ‡§**. Olga Me 1046–1060. https://doi.org/10.1074/mcp.M112.021618.

Nakanishi, M., Rosenberg, D.W., 2013. https://doi.org/10.1007/s00281-012-0342-8.

Nicola, F. De, Castrucci, P., Scarselli, M., n.d. Super-hydrophobic multi-walled carbon nanotube coatings for stainless steel. Nanotechnology 26, 145701. https://doi.org/10.1088/0957-4484/26/14/145701.

Nikshoar, M.S., Khayamian, M.A., Ansaryan, S., Sanati, H., Gharooni, M., Farahmand, L., Rezakhanloo, F., Majidzadeh-A, K., Hoseinpour, P., Dadgari, S., Kiani-M, L., Saqafi, M., Gity, M., Abdolahad, M., 2017. Metas-Chip precisely identifies presence of micrometastasis in live biopsy samples by label free approach. Nat. Commun. 8. https://doi.org/10.1038/s41467-017-02184-x.

Peck, B., Schug, Z.T., Zhang, Q., Dankworth, B., Jones, D.T., Smethurst, E., Patel, R., Mason, S., Jiang, M., Saunders, R., Howell, M., Mitter, R., Spencer-dene, B., Stamp, G., Mcgarry, L., James, D., Shanks, E., Aboagye, E.O., Critchlow, S.E., Leung, H.Y., Harris, A.L., Wakelam, M.J.O., Gottlieb, E., 2016. Inhibition of fatty acid desaturation is detrimental to cancer cell survival in metabolically compromised environments. Cancer Metabol. 1–18. https://doi.org/10.1186/s40170-016-0146-8.

Peter, J.F., Otto, A.M., Wolf, B., 2007. AB R F Enrichment and Detection of Molecules Secreted by Tumor Cells Using Magnetic Reversed-phase Particles and LC-MALDI-TOF-MS, vol. 18. pp. 287–297.

Pol, A., Gross, S.P., Parton, R.G., 2014. Biogenesis of the multifunctional lipid droplet: lipids, proteins, and sites. J. Cell Biol. 204, 635–646. https://doi.org/10.1083/jcb.201311051.

Richens, J.L., Lane, J.S., Bramble, J.P., O'Shea, P., 2015. The electrical interplay between proteins and lipids in membranes. Biochim. Biophys. Acta - Biomembr. 1848 1828–1836. https://doi.org/10.1016/j.bbamem.2015.03.017.

Skotland, T., Sandvig, K., Llorente, A., 2017. Progress in lipid research lipids in exosomes : current knowledge and the way forward. Prog. Lipid Res. 66, 30–41. https://doi.org/10.1016/j.plipres.2017.03.001.

Tirinato, L., Pagliari, F., Limongi, T., Marini, M., Falqui, A., Seco, J., Candeloro, P., Liberale, C., Di Fabrizio, E., 2017. An overview of lipid droplets in cancer and cancer stem cells. Stem Cells Int. 2017. https://doi.org/10.1155/2017/1656053.

Tosch, W., Lanthaler, K., Boote, V., Stretz, D., Robson, G.D., Geiger, E., Drucker, D.B., 2006. Molecular species of phospatidylethanolamine from continuous cultures of Saccharomyces pastorianus syn. carlsbergensis strains. Yeast 23, 75–82. https://doi.org/10.1002/yea.1339.

Triebl, A., Trötzmüller, M., Eberl, A., Hanel, P., Hartler, J., Köfeler, H.C., 2014. Quantitation of phosphatidic acid and lysophosphatidic acid molecular species using hydrophilic interaction liquid chromatography coupled to electrospray ionization high resolution mass spectrometry. J. Chromatogr. A 1347, 104–110. https://doi.org/10.1016/j.chroma.2014.04.070.

Tulloch, A.P., 1985. Mass spectra of pyrrolidides of oxy, hydroxy and trimethylsilyloxy octadecanoic acids. Lipids 20, 652–663. https://doi.org/10.1007/BF02534383.

Wang, D., Dubois, R.N., 2006. Prostaglandins and cancer. Gut 55, 115–122. https://doi.org/10.1136/gut.2004.047100.

Yue, S., Li, J., Lee, S., Lee, H.J., Shao, T., Song, B., Cheng, L., Masterson, T.A., Liu, X., Ratliff, T.L., Cheng, J., 2014. Article cholesteryl ester accumulation induced by PTEN loss and PI3K/AKT activation underlies human prostate cancer aggressiveness. Cell Metabol. 19, 393–406. https://doi.org/10.1016/j.cmet.2014.01.019.

Zandi, A., Gilani, A., Ghafoori fard, H., Koohsorkhi, J., 2019a. An optimized resistive CNT-based gas sensor with a novel configuration by top electrical contact. Diam. Relat. Mater. 93, 224–232. https://doi.org/10.1016/j.diamond.2019.01.020.

Zandi, A., Khayamian, M.A., Saghafi, M., Shalileh, S., Katebi, P., Assadi, S., Gilani, A., Salemizadeh Parizi, M., Vanaei, S., Esmailinejad, M.R., Abbasvandi, F., Hoseinpour, P., Abdolahad, M., 2019b. Microneedle-based generation of microbubbles in cancer tumors to improve ultrasound-assisted drug delivery. Adv. Healthc. Mater 1900613, 1900613. https://doi.org/10.1002/adhm.201900613.

Zhu, Y., Wang, L., Xu, C., 2012. Carbon nanotubes in biomedicine and biosensing. Carbon Nanotub. - Growth Appl. https://doi.org/10.5772/16558.

Zhu, Z., 2017. An overview of carbon nanotubes and graphene for biosensing applications. Nano-Micro Lett. 9, 1–24. https://doi.org/10.1007/s40820-017-0128-6.